Acta Astronautica 214 (2024) 316–323

Contents lists available at ScienceDirect

Acta Astronautica

journal homepage: www.elsevier.com/locate/actaastro

Fragments analysis of an hypervelocity impact experiment on a solar array

L. Olivieri lorenzo [a,*], C. Giacomuzzo [a], A. Francesconi [b]

[a] CISAS G. Colombo, University of Padova, Via Venezia 15, 35131, Padova, PD, Italy
[b] DII/CISAS G. Colombo, University of Padova, Via Venezia 15, 35131, Padova, PD, Italy

ARTICLE INFO

Keywords:
Hypervelocity impact testing
Fragments distribution
Space debris
Solar array

ABSTRACT

A large fraction of spacecraft external surfaces or appendages often consists of solar arrays, which can be subjected to space debris impacts as in the case of the Sentinel 1 A event of August 2016. Therefore, it is of interest to understand how solar arrays respond to hypervelocity impacts and to investigate the generated fragments population. In this context, the University of Padova performed an impact experiment on a solar array consisting in a composite sandwich panel, coated with a Kapton layer, and provided with solar cells: a nylon cylinder of 0.039 g collided with the solar panel at a velocity of 4.86 km/s with an impact angle of 45 deg, detaching a solar cell and damaging the panel structure. More than 4500 fragments larger than 0.2 mm were collected and classified after the impact.

In this paper the impact experiment is described and the fragments analysis is presented in terms of size and shape distributions; a comparison with a test on a composite sandwich panel shows that the distributions are strongly affected by material and manufacturing choices, in particular regarding the fragments generated by delamination.

1. Introduction

Space debris currently present a consistent hazard for spacecraft in Earth orbits [1]; the scientific community is particularly concerned by the increasing launch trend of small satellites and large constellation spacecraft, that can further affect the debris environment [2–4]. The sustainability of Earth orbits is a growing concern, and efforts to lessen the effect of new missions on the debris environment are being developed through both legislation and self-regulation [5,6]; in parallel, old and malfunctioning spacecraft removal is under consideration [7–9] to further reduce the potential sources of new space debris due to collision events [10,11]. However, current trends suggest that both the number of objects resident in Earth orbits and the probability of impact events will increase in the next future [12,13].

Among the most recent known space debris collisions, on August 23rd, 2016, a solar panel of the Sentinel 1 A Earth observation satellite was hit by a small objects, causing a sudden power loss and a small deviation from the nominal attitude and orbit. An on-board camera allowed detecting an indentation on the solar array [14] and ground observations detected at least 8 debris generated by the event [15,16]. A first reconstruction of the impact [14] suggests that the collision occurred at 11 km/s at an angle of about 45 deg with respect to the panel normal direction; the projectile mass turned out to be ~0.2 g, equivalent to an aluminium-alloy sphere with diameter equal to 5.1 mm. However, the authors observe that the impactor was likely non-spherical (e.g. disk-shaped).

Literature data on the response of solar panels to space debris impacts is relatively scarce, with few works mainly focusing on the effect of the collision on spacecraft attitude [17] and on solar cells degradation [18], including the generation and effects of plasma [19–21]. Additional works include a study about ejecta product model [22], which validation was based on the post-flight analysis of the damage on solar arrays exposed to the space environment in the EuReCa mission [23], and a detailed analysis of impact craters to determine the residues of solar cells ejecta, both on ground and on the recovered solar arrays of the Hubble Space Telescope [24,25]. To better understand the differences among collisions on solar panels and on composite and Aluminium honeycomb sandwich panels, Masuyama performed a campaign of impact tests and analysed the craterisation of a witness plate [26]; results suggest that brittle material of the solar cells can generate a larger number of ejecta with respect to the other targets, in particular for collisions on the panel back face (i.e. the cells are fragmented by the debris cloud propagated and expanded inside the panel structure). However, no experimental data is available on the number and characteristics of fragments

* Corresponding author.
E-mail addresses: lorenzo.olivieri@unipd.it (L. Olivieri lorenzo), cinzia.giacomuzzo@unipd.it (C. Giacomuzzo), alessandro.francesconi@unipd.it (A. Francesconi).

https://doi.org/10.1016/j.actaastro.2023.10.044
Received 29 August 2023; Received in revised form 26 September 2023; Accepted 28 October 2023
Available online 3 November 2023

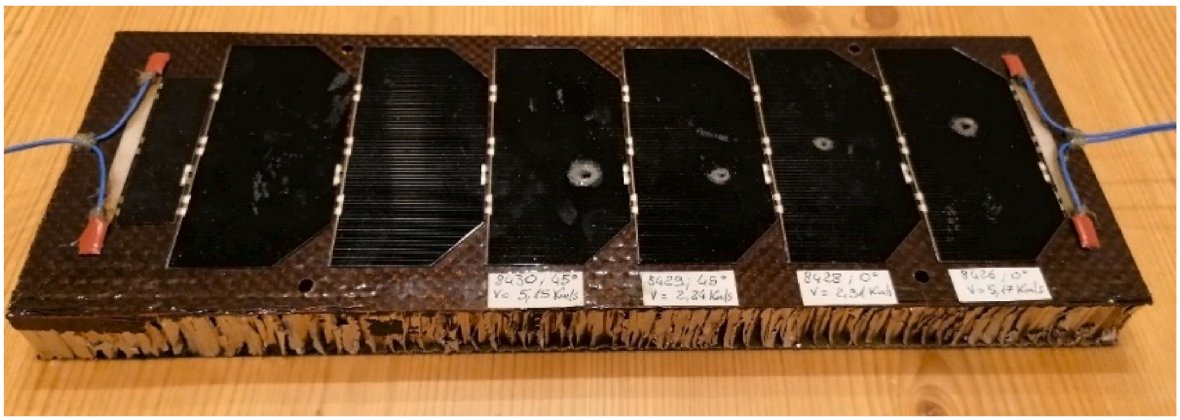

Fig. 1. Sample for test group C1 – sandwich panel with solar cells (representative of Sentinel-1A solar panel).

Table 1
Main parameters of the sample used for impact testing.

Parameter	Test sample
Cell and cover glass thickness	400 μm
Skins thickness	0.75 mm
Core thickness	18.4 mm
Core geometry	Al HC with 3/16″ exagonal cells
Notes:	Kapton insulation layer on front skin

generated by an impact on a solar array; this investigation is still important, as solar arrays often represent a large fraction of satellites cross section and in case of collisions they can strongly contribute to the generation of new space debris. In this context, in the framework of a contract awarded by the European Space Agency to the Italian enterprise SpaceDys [27], the University of Padova is investigating the fragmentation response of simple [28,29] and complex [30,31] targets subjected to hypervelocity impacts; the collected data is employed to better understand fragmentation phenomena and characterize the debris environment in size classes not directly detectable from ground telescopes. Among the tests executed in CISAS Hypervelocity Impact Facility [32], a solar array consisting in a composite sandwich panel, a Kapton coating, and solar cells was subjected to an impact test; the fragments generated by the collision were collected and classified. In this paper the experiment is described and the fragments analysis is presented in terms of size and shape distributions; a comparison with an impact test on a composite sandwich panel shows that the shape of the fragments is strongly affected by material and manufacturing choices, in particular regarding the fragments generated by delamination.

2. Test setup and impact test

Fig. 1 shows the sample solar panel subjected to the test; a summary of its main characteristics is reported in Table 1. It consists of a composite sandwich panel with an aluminium core and two single ply carbon-fibre reinforced panels (CFRPs) acting as skins; an insulation

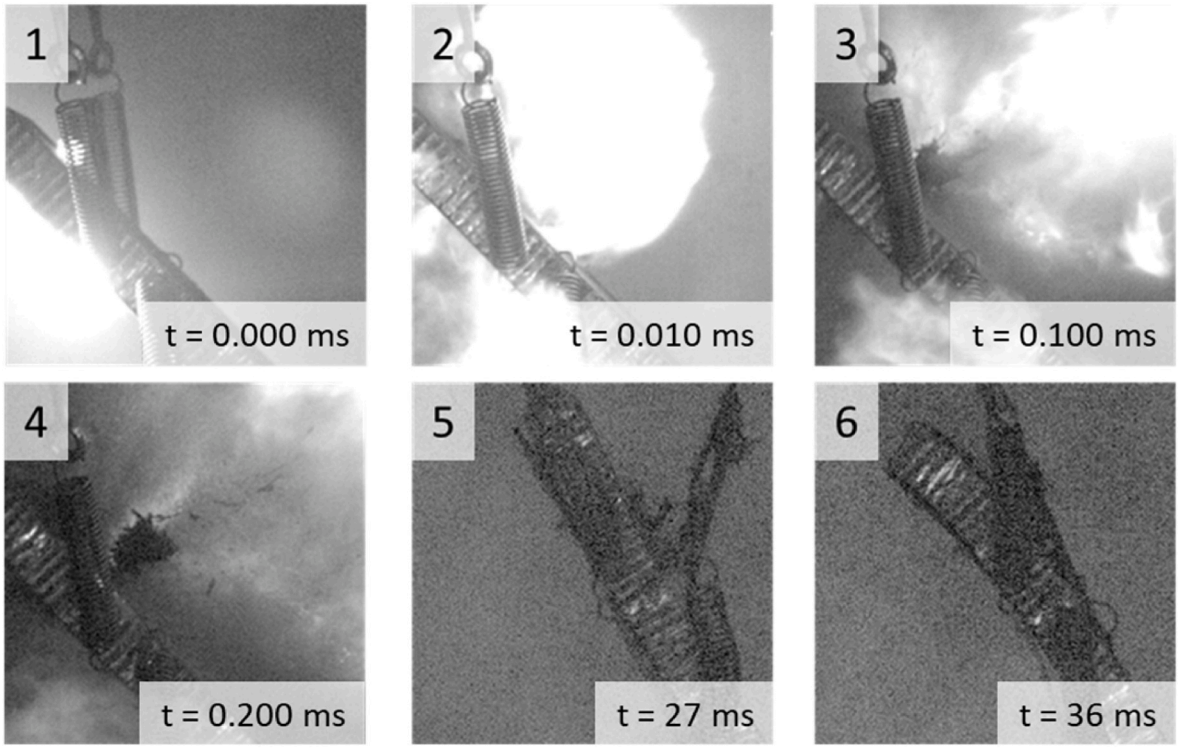

Fig. 2. Frames from the impact sequence.

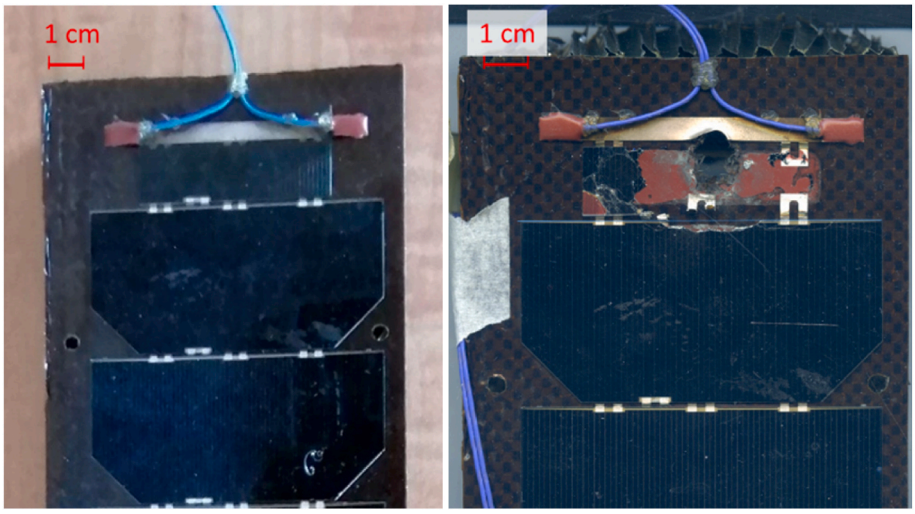

Fig. 3. Target front face before (left) and after (right) the impact.

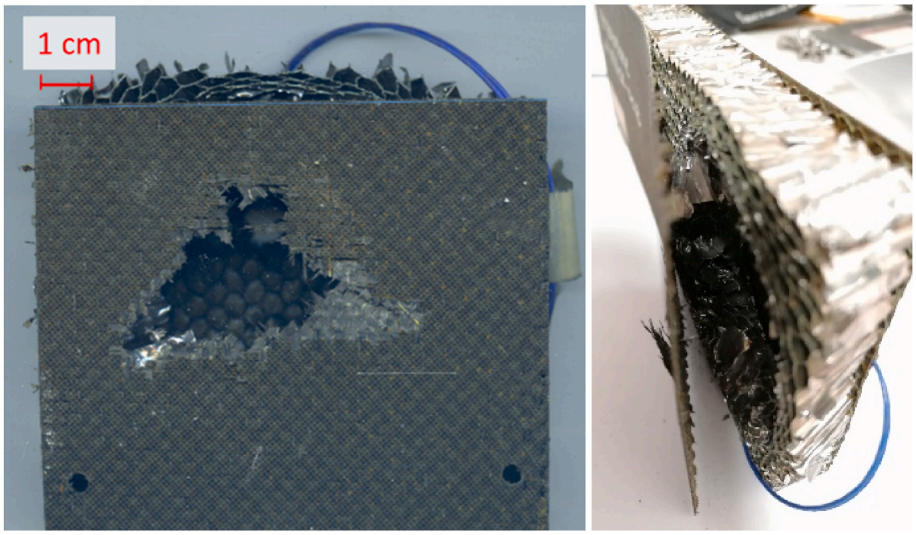

Fig. 4. Target back face (left) and honeycomb core (right) damage from the impact.

layer in Kapton is placed between the upper CFRP skin and the solar cell. While part of the sample was previously subjected to non-destructive impact tests, more than one third of the solar panel was intact (on the left in figure): the experiment was performed on this undamaged section.

The impact test was carried out at the CISAS Hypervelocity Impact Facility using a two-stage Light-Gas Gun (LGG), capable of accelerating projectiles up to 100 mg at a maximum speed of 5.5 km/s [33–35]. The target was hanged in a dedicated box with soft walls (polystyrene foam and plywood) to collect the generated fragments; the box was then installed inside the LGG impact chamber (see Refs. [28,31] for the collection box description). The projectile consisted in a Nylon cylinder with diameter 4.72 mm and height 4 mm, with a mass of 0.039 g; it impacted the panel at a velocity was 4.86 km/s and with an angle of 45 deg with respect to the sample normal. Fig. 2 shows six frames from the high-speed camera recording the impact; the projectile comes from the left side. It can be noted that after the collision (frames 1 and 2) a large fragment detaches from the back face with a cloud of smaller objects (frames 3 and 4); after that, large bending oscillations are visible both on the panel and on a partially detached back face (frames 5 and 6).

Fig. 3 shows the target front face before (left) and after (right) the impact. The small solar cell on the top of the panel fully detached; the perforation hole is small and irregular (about 11.5 mm in diameter).

Fig. 4 shows the back face of the target; in this case, the damage on the skin is larger than the front face one, about 33.5 mm × 41.5 mm. The whole skin partially detached, showing that the damage on the honeycomb core is still larger, up to about 80 mm in diameter; the internal cells are completely fragmented in the central section of the damaged volume and partially deformed on its boundaries.

3. Fragments collection and classification

Before the test, the solar panel and the projectile were weighed. After the test, the generated fragments were extracted from the collision box and collected for their characterization following the procedures reported in Refs. [28,31]. In summary, a first qualitative assessment led to the collection of the largest fragments (see Fig. 5, top left), that were individually weighed and characterized; the remainder of the fragments were mechanically sifted in five different size classes (larger than 3 mm, between 2 mm and 3 mm, between 1 mm and 2 mm, between 0.5 and 1 mm, and below 1 mm) and each class was weighed. Fig. 5 shows the recovered fragments; these images were acquired with a planar photographic scanner set at 600 dpi resolution (0.0423 mm/pixel) and were then employed for automatic analysis of fragments size; details on the

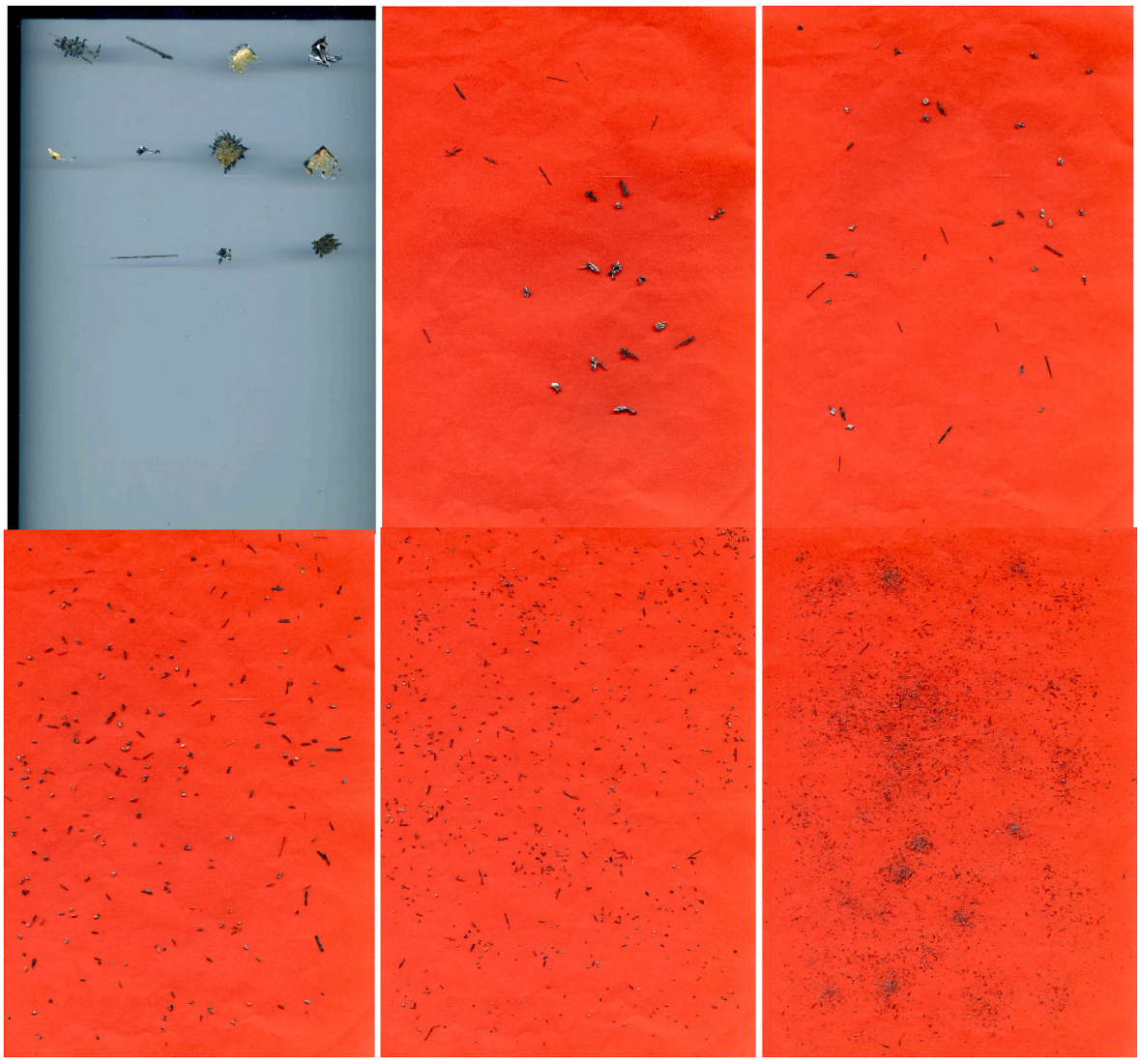

Fig. 5. Example of recovered fragments: from top to bottom, left to right, largest fragments, classes >3 mm, 2–3 mm, 1–2 mm, 0.5–1 mm, <0.5 mm.

Table 2
Mass information for tests in the group C1, with mass collection efficiency.

Target mass before impact, g	Projectile mass, g	Target mass after impact, g	Δ mass, g	Collected mass, g	Mass collection efficiency
116.609	0.093	114.468	2.234	1.394	62.4 %

software employed for the analysis can be found in Ref. [31].

The main mass parameters of this test are listed in Table 2 and include the Δ mass (difference between the target plus projectile mass before the impact and the target mass after the impact), the mass collected from the test, and the mass collection efficiency (ratio between collected mass and Δ mass). The collection efficiency is about 62 %, in line with other tests performed on sandwich panels [28,30].

4. Results

The main results of the analysis are addressed in this section, and the fragment distributions are shown and evaluated in comparison to a reference test on a CFRP honeycomb sandwich panel [30].

4.1. Size and mass

Table 3 shows the cumulative mass and the number of detected

Table 3
Cumulative mass and number of detected fragments for each class.

Largest fragments		L > 3 mm		2 mm < L <3 mm		1 mm < L <2 mm		0.5 mm < L <1 mm		L < 0.5 mm		N_{TOT}	m_{TOT}
Mass, g	N	Mass, g	N	Mass, g	N	Mass, g	N	Mass, g	N	Mass, g	N		
0.733	11	0.064	22	0.055	42	0.145	245	0.160	818	0.237	3563	4701	1.394

More than 4700 fragments were collected and recognized by the image analysis software; the 11 largest ones represent more than half of the total weight (52.6 %); they are generated by the skins surface and the detached solar cell.

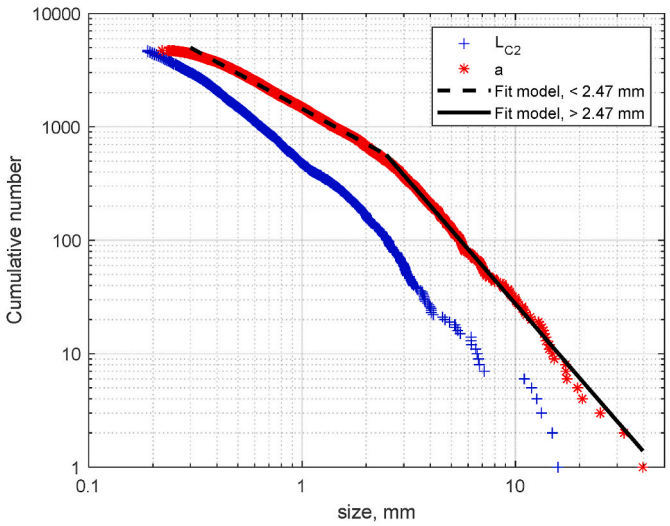

Fig. 6. Fragments cumulative number distributions in function of characteristic length (left) and largest dimension (right).

Table 4
Fit model main parameters.

Model	p_1	p_2	R^2
<2.47 mm	−1.03	3.16	0.995
>2.47 mm	−2.17	3.61	0.996

fragments for the five size classes; the mass lost during sifting and weighing procedures is negligible.

4.2. Characteristic length distribution

The fragments size cumulative distributions are reported in this section in terms of their largest size and characteristic length [36]. Due to the planar scanner employed in the data acquisition, only the 2-D cross-section of the fragments was acquired; for this reason in this work, a 2-D characteristic length is employed in this work, defined as the average of the lengths of the minor (L_{MIN}) and major (L_{MAX}) axes of the ellipse with the same normalized second central moments as the detected fragment. This allows presenting results without assumptions on the fragments third dimension, with negligible effect on the trend or shape of cumulative distributions. For a full description of the bi-dimensional characteristic length and the comparison with the standard formulation, refer to Refs. [28,31].

Fig. 6 shows the cumulative distributions of the scanned fragments in function of their 2-D characteristic length (L_{C2}, blue) and largest dimension (a, red). It can be noted that the two distributions in the log-log space are similar to two-line piecewise curves, with the transition point located between 2 mm and 3 mm for the largest dimension. A fit model is therefore proposed in the following form:

$$\log_{10} N = p_1 \cdot \log_{10} a + p_2 \tag{1}$$

where N is the cumulative number of fragments, a is the largest size, and p_1 and p_2 respectively the slope and the intercept of the model. The transition point was located at 2.47 mm by finding the best fitting piecewise model, i. e the one for which the average of the coefficients of determination of the two lines is maximized. The values of slope and intercept for the two lines of the model are listed in Table 4, as well as the coefficients of determination.

The two different slopes of the model, with a ratio $p_{1,<2mm}/p_{1,>2mm}$ of about 0.5, suggest that different phenomena may affect the generation of fragments larger and smaller than 2.47 mm. It can be hypothesized that the 2.47 mm threshold represents the transition from the objects detached from the solar panel to the finer fragments generated in the target volume that is directly affected by the projectile and its debris cloud; additional tests might be required to identify with a statistical significance the position of this threshold.

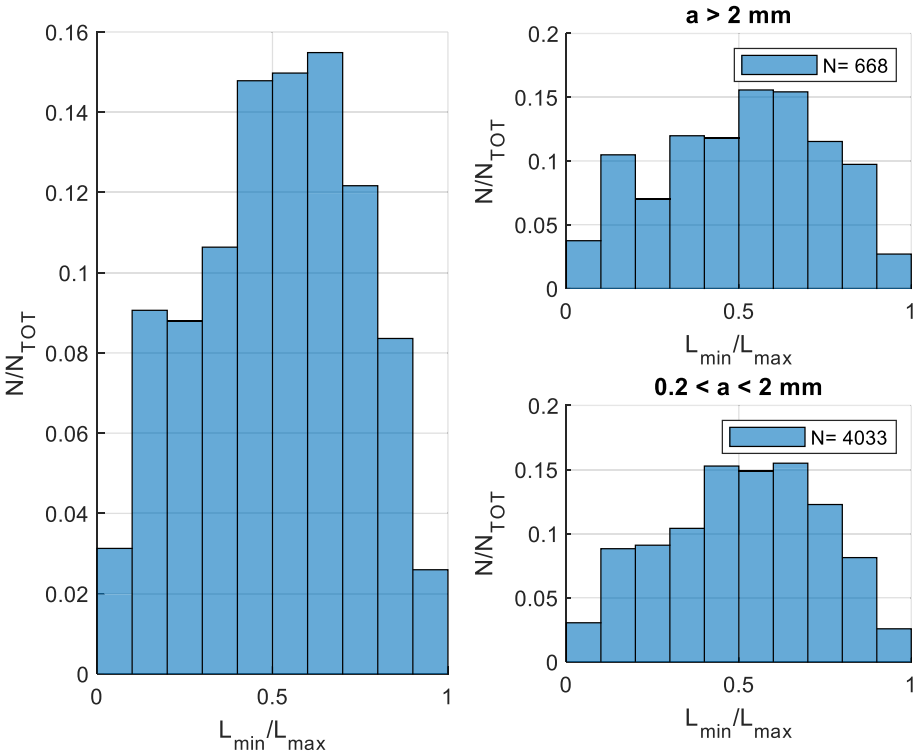

Fig. 7. Fragments shape distribution.

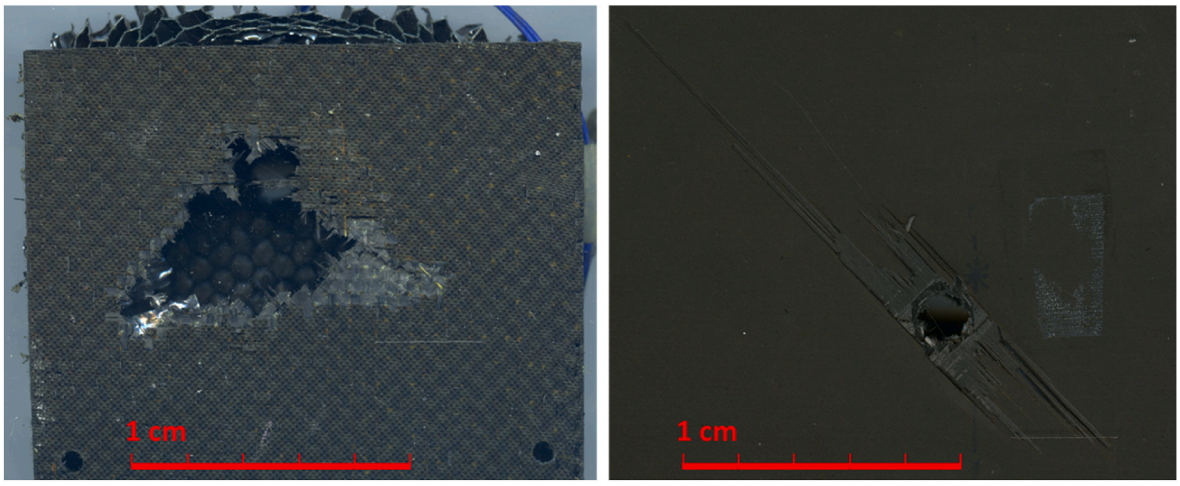

Fig. 8. Comparison of back face crater for solar array (left) and CFRP-skin sandwich panel (right).

4.3. Shape distribution

In this subsection, the shape of the detected fragments is presented in terms of the ratio between their smaller and larger dimensions L_{MIN}/L_{MAX}.

Fig. 7 shows the shape distributions for this test, both for the full fragments population and the two size classes larger and smaller than 2 mm. It can be noted that the mode of the shape ratio is about 0.7 (slightly elliptical or rectangular fragments), but the fragments are well distributed in all shape classes. In addition, the difference between size classes distributions is negligible; this suggests a uniform distribution of the solar array materials in all classes. This result is interesting if compared with data in literature; as reference, the fragmentation test performed on aluminium simple plates [28] and sandwich panels [30] showed a consistent influence of the size class on the shape distribution. A more detailed comparison with sandwich panels is reported in the next subsection.

4.4. Comparison with CFRP sandwich panel

In this subsection, the experimental distributions obtained from the solar panel are compared with results from a hypervelocity test performed on a honeycomb sandwich panel with CFRP skins [30]. The objective of this comparison is to evaluate if the fragmentation phenomena for a solar panel can be compatible with a sandwich plate one; this would simplify both the testing activities (CFRP panels procurement could be easier and less expensive for extensive experimental campaigns) and the fragmentation modelling and simulations.

Both test samples present a similar thickness of (respectively 0.5″ and 0.75″), but the compared sandwich panel has thicker skins (2.3 mm), with plies with directional fibres and no Kapton layer. The test envisaged a 2.3 mm spherical aluminium projectile (mass of 0.039 g) impacting the panel at a velocity of 4.80 km/s, normally to the surface; the impact energy is 392 J, about one third of the solar panel one. Despite the different structure and impact geometry, the sandwich panel generated a number of fragments comparable to the solar panel (respectively 4870 and 4701). In the following lines, similarities and differences between the two experiments are discussed.

Fig. 8 compares the damage on the two panels back faces. For the solar panel the perforation area is wider (about 33.5 mm × 41.5 mm) and more irregular with respect to the sandwich panel (quasi-circular hole with a diameter 9.2 mm); however, the surface delamination of the solar panel is limited, while the first ply of the sandwich panel show long and narrow detachments in the direction of the fibres. In fact, the back face of the solar panel shows a weave pattern, while the sandwich panel skin consists of overlapped plies with all the fibres oriented alternatively at +45 and −45 deg; it is clear that the fabrication method strongly influences the generation of fragments due to delamination.

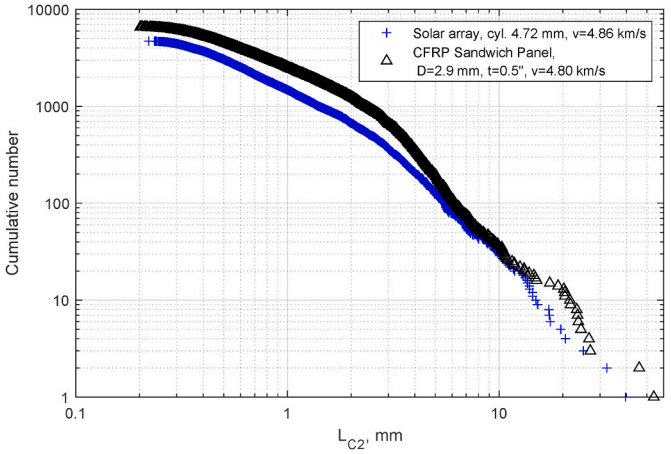

Fig. 9. Comparison of fragments cumulative number distributions for solar panel (blue plus marker) and sandwich panel (black triangles). (For interpretation of the references to colour in this figure legend, the reader is referred to the Web version of this article.)

Fig. 9 compares the solar panel largest dimension a cumulative distribution (blue markers) with the one from the CFRP-skin sandwich panel (black triangles). In general, despite the higher impact energy, the solar panel distribution is always below the sandwich panel one, suggesting that its structural configuration (thinner skins with weave pattern, presence of a Kapton layer) is less prone to generate fragments. It can be observed that for sizes smaller than 10 mm the two curves have a similar trend, with the sandwich panel generating a slightly larger number of objects. For larger sizes, the curve shapes change and sandwich panel generates larger fragments than the solar panel: as reference, at 20 mm the cumulative numbers are respectively 13 and 3. This is due to the surface delamination of the sandwich panel CFRP skins, which generates long and narrow needle-like objects; on the contrary, the solar panel is less affected by delamination. It shall be underlined that these fragments represent the largest mass fraction of the ejecta; even small differences in their number can be relevant when considering their effect on the debris environment and the impact risk.

Fig. 10 shows fragments shape distributions for the solar panel (blue) and the sandwich panel (brown). The general distribution (left), covering all size classes, shows that the sandwich panel generates more

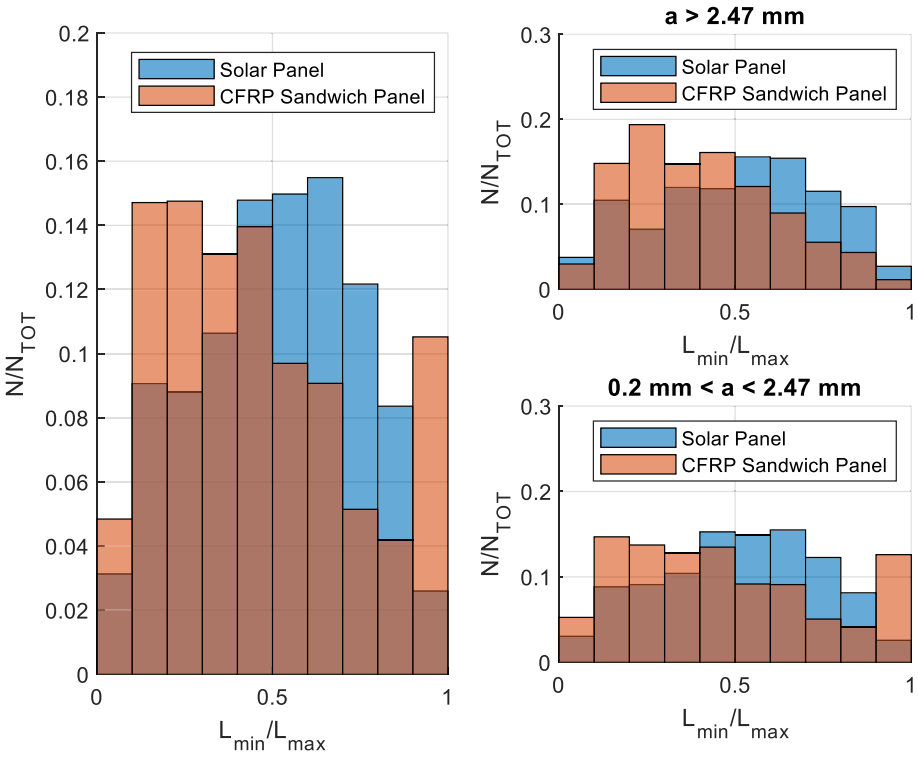

Fig. 10. Comparison of solar panel (blue) and sandwich panel (brown) fragments shape distributions. (For interpretation of the references to colour in this figure legend, the reader is referred to the Web version of this article.)

needle-like object (shape ratio $L_{MIN}/L_{MAX} < 0.5$) and few round object (shape ratio close to one); this is a substantial difference with respect to the solar panel, whose fragments shapes lie mainly in the range 0.4–0.8. The shape distributions divided for size classes (right) better highlight this trend, with a minimum size limit at 0.2 mm, to avoid rounding approximations on the smallest detected particles. In fact, in the largest fragments class ($a > 2.47$ mm) the sandwich panel shows a peak around 0.2, caused by the delamination fragments with long and narrow shapes, that is not present for the solar panel. For smaller fragments this trend is still recognizable, but the number of needle-like objects in lower; however, in this case the sandwich panel generates also the majority of the round fragments (shape ratio close to one). It can be concluded that, despite showing similar size distribution curves, the two experiments strongly differ in shape distributions; this is related to the different geometry and manufacturing of the sandwich panel.

5. Conclusions

An impact test at 4.86 km/s performed on a 0.75″ solar panel with a cylindrical projectile was described in this paper and the analysis of the fragments generated by the event was presented. More than 4700 fragments were collected and classified, obtaining size and shape distributions.

Fragments size distributions show a trend that can be approximated with a two-line piecewise model; the threshold between the two branches is at about 2.47 mm. This threshold represents the transition from the objects detached from the solar panel to the finer fragments generated in the target volume that is directly affected by the projectile and its debris cloud. A fitting model is developed, with a coefficient of determination larger than 0.99 for both lines.

The shape distribution presents a peak at about 0.7 (slightly elliptical or rectangular fragments), but the fragments are well distributed in all shape classes. In addition, the influence of fragments size on the shape is negligible; this suggests a uniform distribution of the solar array materials in all classes.

Distribution curves were compared with results from a test on a CFRP-skin honeycomb with similar thickness but thicker skins. Despite the lower impact energy (about one third of the solar panel test), the sandwich panel generates about the same number of fragments and is affected by surface delamination: distribution curves show more objects larger than 10 mm and with aspect ratios around 0.2, indicating the presence of long and narrow needle-like fragments. This consistent difference is mainly related to the two samples manufacturing: the solar panel employ thin skins with fibres in a weave pattern, reinforced by a Kapton layer, while the sandwich panel skins consist of overlapped plies with ply fibres oriented in the same direction.

In conclusion, it is shown that the fragmentation process of complex targets such as solar panels is strongly affected by materials and manufacturing choices; dedicated numerical or statistical model shall include this information to predict reliable fragments distributions.

Declaration of competing interest

The authors declare that they have no known competing financial interests or personal relationships that could have appeared to influence the work reported in this paper.

Acknowledgments

The authors wish to thank Mr. Francesco Babolin and Mr. Nicola Stocco for their support in targets preparation and data collection. This work is realized in the framework of ESA contract n. TDE-T711-603SD “Exploiting numerical modelling for the characterization of collision break-ups”.

References

[1] Tim Maclay, Darren Mcknight, Space environment management: framing the objective and setting priorities for controlling orbital debris risk, J. Space Safety Engin. 8 (1) (2021) 93–97.

[2] Vitali Braun, Small satellite constellations and end-of-life deorbit considerations, in: Handbook of Small Satellites: Technology, Design, Manufacture, Applications, Economics and Regulation, 2019, pp. 1–23.
[3] Giacomo Curzi, Dario Modenini, Paolo Tortora, Large constellations of small satellites: a survey of near future challenges and missions, Aerospace 7 (9) (2020) 133.
[4] L. Olivieri, A. Francesconi, Large constellations assessment and optimization in LEO space debris environment, Adv. Space Res. 65 (1) (2020) 351–363.
[5] Daniel L. Oltrogge, Ian A. Christensen, Space governance in the new space era, J. Space Safety Engin. 7 (3) (2020) 432–438.
[6] Rada Popova, Volker Schaus, The legal framework for space debris remediation as a tool for sustainability in outer space, Aerospace 5 (2) (2018) 55.
[7] Pietro Tadini, et al., Active debris multi-removal mission concept based on hybrid propulsion, Acta Astronaut. 103 (2014) 26–35.
[8] Mark C Priyant, Surekha Kamath, Review of active space debris removal methods, Space Pol. 47 (2019) 194–206.
[9] Z. Pavanello, et al., Combined control and navigation approach to the robotic capture of space vehicles, 72nd Int. Astronaut. Congress (IAC (2021) 2021.
[10] Si-yuan Ren, et al., Satellite Breakup Behaviors and Model under the Hypervelocity Impact and Explosion: A Review, Defence Technology, 2022.
[11] Nicholas L. Johnson, et al., The characteristics and consequences of the break-up of the Fengyun-1C spacecraft, Acta Astronaut. 63 (1) (2008) 128–135.
[12] Carmen Pardini, Luciano Anselmo, Evaluating the impact of space activities in low earth orbit, Acta Astronaut. 184 (2021) 11–22.
[13] Carmen Pardini, Luciano Anselmo, Using the space debris flux to assess the criticality of the environment in low Earth orbit, Acta Astronaut. (2022).
[14] H. Krag, et al., A 1 cm space debris impact onto the sentinel-1a solar array, Acta Astronaut. 137 (2017) 434–443.
[15] https://www.space-track.org/.
[16] M.E. Sorge, G. Peterson, J. McVey, Forensic analysis of on-orbit debris generation events, in: Proc. 7th, ECSD, 2017. OTR 513.
[17] A.V. Sedelnikov, Evaluation of the level of microaccelerations on-board of a small satellite caused by a collision of a space debris particle with a solar panel, Jordan J. Mechan. Industr. Engin. 11 (2017) 2.
[18] Y. Akahoshi, et al., Influence of space debris impact on solar array under power generation, Int. J. Impact Eng. 35 (12) (2008) 1678–1682.
[19] Yuki Mando, et al., "Investigation on Sustained Discharge of Satellite's Power Harness Due to Plasma from Space Debris Impact." Hypervelocity Impact Symposium, vol. 883556, American Society of Mechanical Engineers, 2019.
[20] Jean-Michel Siguier, et al., Secondary arcing triggered by hypervelocity impacts on solar panel rear-side cables with defects—comparison with laser impacts, IEEE Trans. Plasma Sci. 45 (8) (2017) 1880–1886.
[21] K. Fereydooni, A.I. Evans, N. Lee, S. Close, Plasma production and composition from hypervelocity impacts on solar cell cover glass, Int. J. Impact Eng. 169 (2022), 104325.
[22] M. Rival, J.C. Mandeville, Modeling of ejecta produced upon hypervelocity impacts, Space Debris 1 (1) (1999) 45–57.
[23] K.G. Paul, E.B. Igenbergs, L. Berthoud, Hypervelocity impacts on solar cells—observations, experiments, and empirical scaling laws, Int. J. Impact Eng. 20 (6–10) (1997) 627–638.
[24] G. Graham, A. Kearsley, M. Grady, I. Wright, The Rapid Identification of Impact Residues in the Solar Array Panels of the HST by Digitised Back-Scattered Electron and X-Ray Elemental Imaging. In Second European Conference on Space Debris, Organised by ESA, Held 17-19 March, 1997, ESOC, Darmstadt, Germany (1997), ESA-SP 393, vol. 393, 1997, p. 183.
[25] G.A. Graham, A.T. Kearsley, M.M. Grady, I.P. Wright, M.K. Herbert, J.A. M. McDonnell, Natural and simulated hypervelocity impacts into solar cells, Int. J. Impact Eng. 23 (1) (1999) 319–330.
[26] Masuyama, et al., Feasibility of standardized ejecta evaluation for spacecraft surface materials, Procedia Eng. 58 (2013) 543–549, https://doi.org/10.1016/j.proeng.2013.05.062.
[27] L. Dimare, A. Francesconi, C. Giacomuzzo, S. Cicalo, A. Rossi, L. Olivieri, G. Sarego, F. Guerra, S. Lemmens, V. Braun, Advances in the characterisation of collision break-ups by means of numerical modelling, IAC (2021) 25–29. Dubai.
[28] L. Olivieri, C. Giacomuzzo, A. Francesconi, Experimental fragments distributions for thin aluminium plates subjected to hypervelocity impacts, Int. J. Impact Eng. 170 (2022), 104351.
[29] L. Olivieri, C. Giacomuzzo, A. Francesconi, Analysis of fragment distributions from carbon-fiber-reinforced composite panels subjected to hypervelocity impacts, AIAA J. (2023) 1–9.
[30] L. Olivieri, C. Giacomuzzo, A. Francesconi, Impact fragments from honeycomb sandwich panels, IAC (2022) 18–22. September 2022.
[31] Lorenzo Olivieri, et al., Characterization of the fragments generated by a Picosatellite impact experiment, Int. J. Impact Eng. 168 (2022), 104313.
[32] F. Angrilli, D. Pavarin, M. De Cecco, A. Francesconi, Impact facility based upon high frequency two stage light-gas gun, Acta Astronaut. 53 (3) (2003) 185–189, https://doi.org/10.1016/S0094-5765(02)00207-2.
[33] D. Pavarin, A. Francesconi, Improvement of the CISAS high-shot frequency light-gas gun, Int. J. Impact Eng. 29 (1–10) (2004) 549–562, https://doi.org/10.1016/j.ijimpeng.2003.10.004.
[34] D. Pavarin Francesconi, A. Bettella, F. Angrilli, A special design condition to increase the performance of two-stage light-gas guns, Int. J. Impact Eng. 35 (Issue 12) (December 2008) 1510–1515, https://doi.org/10.1016/j.ijimpeng.2008.07.035.
[35] A. Francesconi, et al., A special design condition to increase the performance of two-stage light-gas guns, Int. J. Impact Eng. 35 (12) (2008) 1510–1515.
[36] N.L. Johnson, P.H. Krisko, J.C. Liou, P.D. Anz-Meador, NASA's new breakup model of EVOLVE 4.0, Adv. Space Res. 28 (9) (2001) 1377–1384.